Supplement of The Cryosphere, 14, 3875–3905, 2020
https://doi.org/10.5194/tc-14-3875-2020-supplement

The Cryosphere Open Access EGU

Supplement of

Temperature and strain controls on ice deformation mechanisms: insights from the microstructures of samples deformed to progressively higher strains at −10, −20 and −30 °C

Sheng Fan et al.

Correspondence to: Sheng Fan (sheng.fan@postgrad.otago.ac.nz)

Contents of this file

Section S1 Sensitivity test of the co-latitude range chosen to quantify cone opening angles

In order to quantify cone opening-angles, we counted the number of *c*-axes that lie at a given angle ("co-latitude") from the compression axis. In practice we counted the *c*-axes between two co-latitudes separated by a co-latitude range and calculated the MUD (multiples of uniform distribution) as a function of co-latitude. We tested the sensitivity of co-latitude range, using values of 2°, 4°, 6° and 8, on the plot of MUD as a function of co-latitude (Fig. S1) for three different samples. The plots are using different co-latitude range are very similar. The 2° range gives rise to significant "spikes" in the distribution that are not apparent in distributions generated with larger co-latitude ranges and probably reflect sparse data sampling. We chose to use a co-latitude range of 4° in data analysis to maximise resolution without having significant problems from spikes related to sparse sampling.

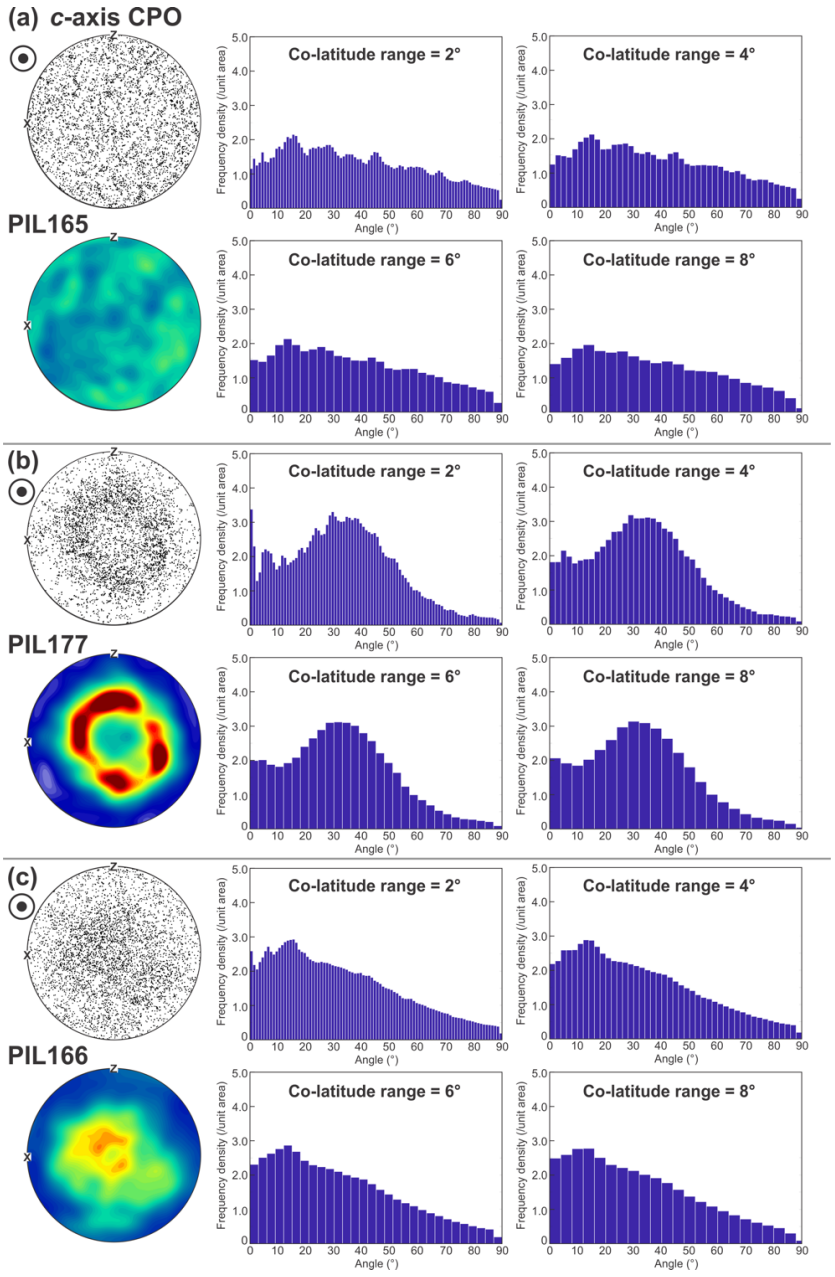

Figure S1. Sensitivity test of co-latitude range on samples of **(a)** PIL 165, characterised by a random CPO, **(b)** PIL177, characterised by a cone-shaped c-axis CPO and **(c)** PIL166, characterised by a narrow-cone-shaped c-axis CPO. For each sample, the upper left box is the point pole figure with 5000 randomly selected points and the lower left box is the corresponding contoured *c*-axis CPO. The centre of the stereonet is parallel to compression. The right part contains MUD distribution as a function of co-latitude with the co-latitude ranges of 2°, 4°, 6° and 8°.

Section S2 Measures of strain: for comparison of our data with other data sets

Published experiments use different ways of calculating strain and strain rate and it is necessary to recalculate values so that the same measurements are being used for comparisons between different studies. Engineering axial strain e, true axial strain ε and octahedral shear strain γ are the most frequently used parameters to quantify the sample deformation in the published literature. Additionally, Hooke and Hudleston (1981) applied natural octahedral unit shear strain, $\bar{\gamma}_{oc}$, to quantify the deformation in the Barnes Ice Cap. For comparison with our data (for Figure 13) e, γ and $\bar{\gamma}_{oc}$ from other studies were converted to ε.

In a uniaxial compression experiment, we define the axial stretch λ (Eq. (S1)) as the ratio of the sample length ($L(t)$) at time t and the initial sample length (L_0).

$$\lambda = \frac{L(t)}{L_0} \quad \text{(Equation S1)}$$

The true axial strain ε, at time t, is given by:

$$\varepsilon = -\ln\left(\frac{L(t)}{L_0}\right) = -\ln(\lambda) \quad \text{(Equation S2)}$$

The engineering axial strain e at time t is given by:

$$e = \frac{L_0 - L(t)}{L_0} = 1 - \lambda \quad \text{(Equation S3)}$$

Therefore, the conversion between true axial strain ε and engineering axial strain e can be expressed as:

$$\varepsilon = -\ln(1 - e) \quad \text{(Equation S4)}$$

The octahedral shear strain γ at time t is given by:

$$\gamma = \frac{1}{3}\sqrt{(\epsilon_1 - \epsilon_2)^2 - (\epsilon_2 - \epsilon_3)^2 - (\epsilon_3 - \epsilon_1)^2}, \quad \text{(EquationS5)}$$

where ϵ_1, ϵ_2 and ϵ_3 represent principle engineering strains at time t. For uniaxial compression, we suppose the horizontal shortening is radially uniform ($\epsilon_2 = \epsilon_3$). Therefore, Eq. (S5) can be simplified as:

$$\gamma = \frac{\sqrt{2}}{3}(\epsilon_1 - \epsilon_3), \quad \text{(Equation S6)}$$

where the principle axial engineering strain ϵ_1 is equal to e. We assume that the sample volume remains unchanged during uniaxial compression. The sample volume V is given by:

$$V = \pi {R_0}^2 L_0 = \pi R(t)^2 L(t), \quad \text{(Equation S7)}$$

where R_0 is the initial sample radius, $R(t)$ is the sample radius at time t. Therefore, $R(t)$ is given by:

$$R(t) = R_0\sqrt{\frac{L_0}{L(t)}}$$
$$= R_0\frac{1}{\sqrt{\lambda}} \quad \text{(Equation S8)}$$

The principle radius engineering strain ϵ_3 is given by:

$$\epsilon_3 = \frac{R_0 - R(t)}{R_0}$$
$$= 1 - \frac{R(t)}{R_0}$$
$$= 1 - \frac{1}{\sqrt{\lambda}}$$
$$= 1 - \frac{1}{\sqrt{1-e}} \quad \text{(Equation S9)}$$

Therefore, Eq. (S6) can be converted to:

$$\gamma = \frac{\sqrt{2}}{3}\left(e + \frac{1}{\sqrt{1-e}} - 1\right) \quad \text{(Equation S10)}$$

In our experiment, the axial displacement remains constant, but the sample length keeps decreasing with time. Consequently, the axial strain rate increases with time. The engineering axial strain rate ($\dot{e}$) is given by:

$$\dot{e} = \frac{d(e)}{dt} \quad \text{(Equation S11)}$$

The relationship between true axial strain rate ($\dot{\varepsilon}$) and engineering axial strain rate ($\dot{e}$) is given by:

$$\dot{\varepsilon} = \frac{d(\varepsilon)}{dt}$$
$$= -\frac{d}{dt}(\ln(1-e))$$
$$= \frac{1}{1-e}\frac{d(e)}{dt}$$
$$= \frac{\dot{e}}{1-e} \quad \text{(Equation S12)}$$

The relationship between octahedral shear strain rate ($\dot{\gamma}$) and engineering axial strain rate ($\dot{e}$) is given by:

$$\dot{\gamma} = \frac{d(\gamma)}{dt}$$
$$= \frac{\sqrt{2}}{3}\frac{d}{dt}\left(e + \frac{1}{\sqrt{1-e}} - 1\right)$$
$$= \frac{\sqrt{2}}{3}\left(\frac{d(e)}{dt} + \frac{d}{dt}\left(\frac{1}{\sqrt{1-e}}\right)\right)$$

$$= \frac{\sqrt{2}}{3}\left(1 + \frac{1}{2(1-e)^{\frac{3}{2}}}\right)\frac{d(e)}{dt}$$

$$= \frac{\sqrt{2}}{3}\left(1 + \frac{1}{2(1-e)^{\frac{3}{2}}}\right)\dot{e} \quad \text{(Equation S13)}$$

Based on Hooke and Hudleston (1981), the relation between $\bar{\gamma}_{oc}$ and principle cumulative longitudinal strain, ϵ_2, horizontal strain, ϵ_3 and vertical strain, ϵ_1 is:

$$\bar{\gamma}_{oc} = \frac{2}{3}[(\epsilon_1 - \epsilon_2)^2 + (\epsilon_2 - \epsilon_3)^2 + (\epsilon_3 - \epsilon_1)^2]^{\frac{1}{2}}. \quad \text{(Equation S14)}$$

For uniaxial compression, $\epsilon_2 = \epsilon_3$. Therefore, Eq. (S14) can be simplified as:

$$\bar{\gamma}_{oc} = \frac{2\sqrt{2}}{3}(\epsilon_1 - \epsilon_3), \quad \text{(Equation S15)}$$

where $\epsilon_1$equals to e. We suppose the ice volume remains unchanged during uniaxial compression. Combine Eq. (S15) and Eq. (S9), and Eq. (S15) can be converted to:

$$\bar{\gamma}_{oc} = \frac{2\sqrt{2}}{3}\left(e + \frac{1}{\sqrt{1-e}} - 1\right) \quad \text{(Equation S16)}$$

Section S3 An estimate of the proportion of "small" grains that are probably a cut through larger grains

For each EBSD map, we measured the lengths of 1-D segments between grain boundaries along a randomly placed line (Fig. S2(a)). Figure S2(b) shows graphs of the lengths of intercept segments and corresponding area equivalent diameters (grain sizes) of the grain that contains each segment. The lengths of intercept segments are generally close to or shorter than the sizes of corresponding grains. The graphs have the threshold grain size to separate "big" and "small" grains in 2-D overlain. Table S1 summarises the statistics of the line intercepts. The percentage of real "small" grains is calculated as the number of 2-D "small" grains divided by number of 1-D line segments shorter than grain size threshold. This percentage of real "small" grains is generally larger at a colder temperature or a higher strain (Table S1, Fig. S3).

Table S1 Statistics of line intercepts

Sample number	T (°C)	True axial strain (ε)	Grain size threshold (μm)	Number of grains along the line	Total length of line (μm)	[1] % of real 2-D "small" grains	% of grains having more than 1 intercept
PIL176	-10	0.03	101	31	4291	20%	3%
PIL163		0.05		77	7253	31%	5%
PIL178		0.08		39	4617	22%	5%
PIL177		0.12		50	4809	21%	4%
PIL007		0.19		128	11030	43%	6%
PIL254	-20	0.03	66	28	4024	44%	0%
PIL182		0.04		43	4613	30%	7%
PIL184		0.08		53	4323	32%	8%
PIL185		0.12		59	4516	53%	8%
PIL255		0.20		73	2905	76%	10%
PIL165	-30	0.03	61	70	8290	28%	4%
PIL162		0.05		73	7014	33%	4%
PIL164		0.07		61	4471	51%	7%
PIL166		0.12		82	6967	77%	0%
PIL268		0.21		44	3820	64%	6%

[1] $\%\ of\ real\ 2-D\ "small"\ grains = \frac{Number\ of\ segments\ in\ 2-D\ \text{small}\ grains}{Number\ of\ segments\ shorter\ than\ grain\ size\ threshold} \times 100$

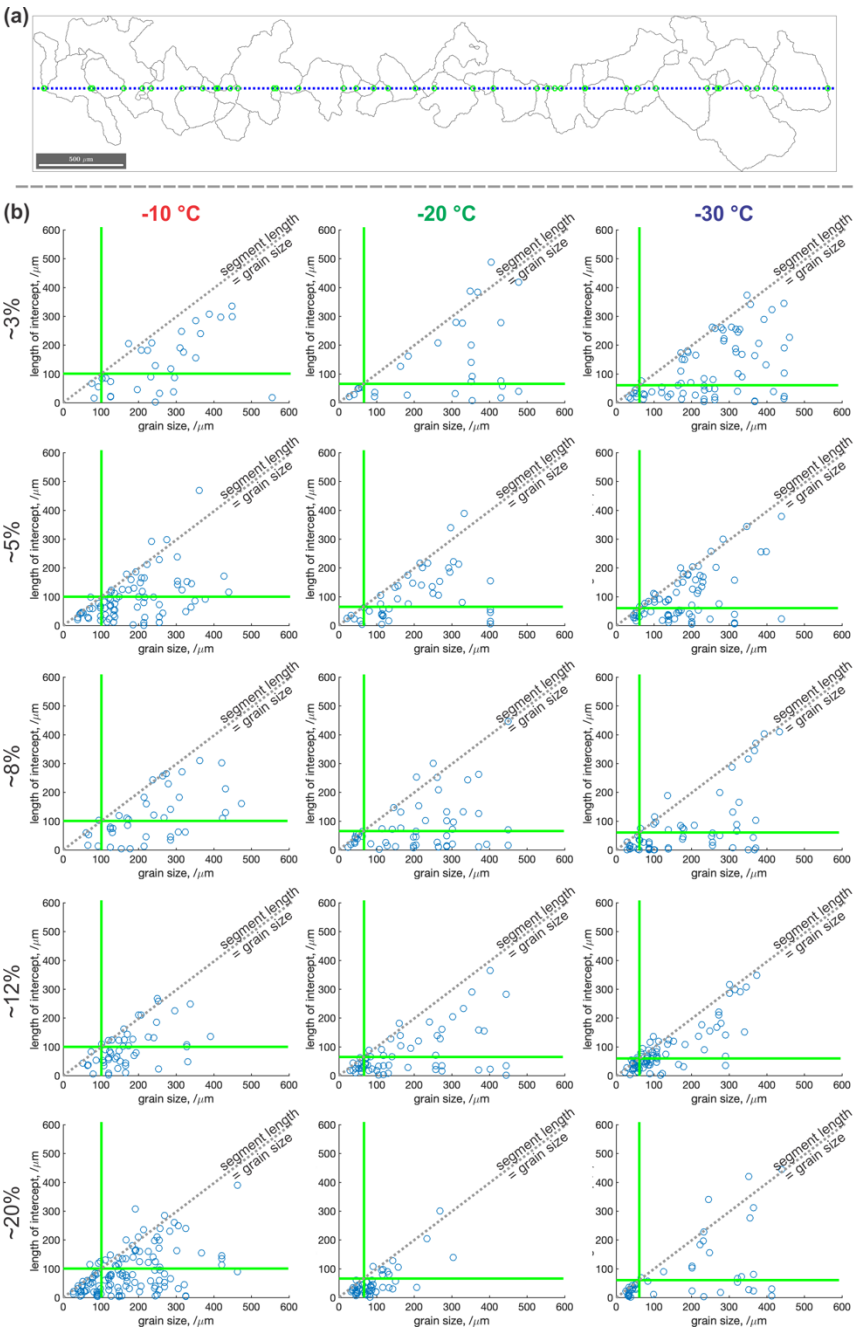

Figure S2. (a) Example of a measurement line (blue dashed line) superposed on a 2-D grain microstructure. The intersections between the line and grain boundaries are marked with green circles. **(b)** Plots of the lengths of intercept segments and corresponding area equivalent diameters (grain sizes). Green lines mark the "small" to "big" threshold grain sizes.

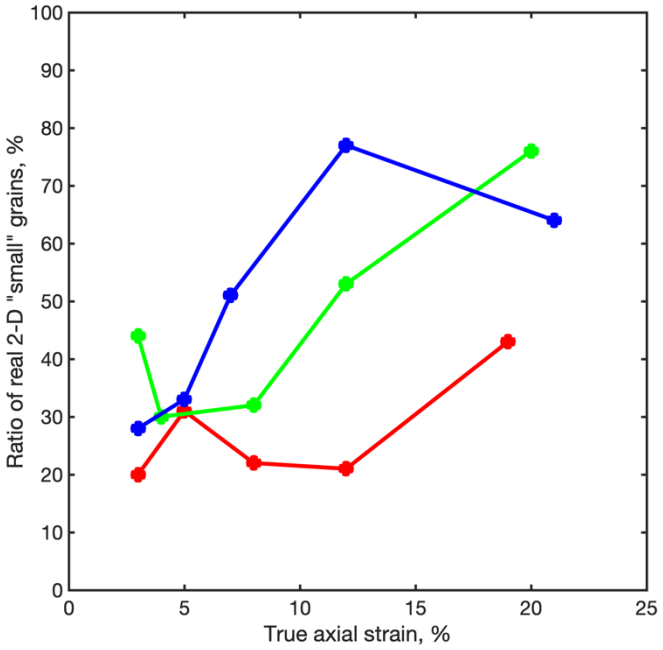

Figure S3. Ratio of real 2-D “small” grains, i.e. number of 2-D “small” grains divided by number of line segments that are shorter than grain size threshold, as a function of true axial strain for samples deformed at -10 °C (red line), -20 °C (green line) and -30 °C (blue line).

Section S4 Estimation of the number of grains in a 2D map that belong to the same grain in three dimensions

EBSD data allows us to compare full crystal orientations so that multiple 2-D slices through the same irregular 3-D grain can be identified. We calculated the misorientation between each grain in a 2-D EBSD map and all the other grains within a distance of 1000 µm (1 mm) from the grain centre. The mean orientation of each grain is used for the calculation. All grains with a misorientation from the first grain of less than 10° are counted as the same grain.

Table S2 Summarise of statistics of grains with mean misorientation differences lower than 10° in 2-D EBSD map

Sample number	T	Strain	[1]Area (μm^{-2})	Total num-ber of grains	[2]Number of non-unique grains	Average [#]co-ordination of non-unique grains	[3]Number of unique grains	[4]Number of "distinct" grains	[5]Percentage of unique grains	[6]Percentage of repeat counted grains	[7]Number density of "distinct" grains (μm^{-2})	[8] Number density of "distinct" grains as ratio to starting material
Undeformed	-	-	1.19E+08	1242	90	2.61	1152	1186	97.09	2.91	9.97E-06	1.00
PIL176	- 10	0.03	1.81E+07	694	190	2.3	504	587	85.92	14.08	3.24E-05	3.25
PIL163		0.05	2.40E+07	1494	567	2.66	927	1140	81.30	18.70	4.75E-05	4.76
PIL178		0.08	1.94E+07	1028	447	2.79	581	741	78.38	21.62	3.82E-05	3.83
PIL177		0.12	1.98E+07	1507	730	3.04	777	1017	76.39	23.61	5.14E-05	5.15
PIL007		0.19	1.96E+07	1789	844	3.02	945	1224	77.18	22.82	6.25E-05	6.27
PIL254	- 20	0.03	1.31E+07	903	253	2.44	650	754	86.24	13.76	5.75E-05	5.77
PIL182		0.04	1.99E+07	907	211	2.24	696	790	88.08	11.92	3.97E-05	3.98
PIL184		0.08	1.85E+07	1157	458	2.6	699	875	79.87	20.13	4.73E-05	4.74
PIL185		0.12	2.00E+07	3023	1425	2.88	1598	2093	76.36	23.64	1.05E-04	10.49
PIL255		0.20	1.27E+07	3057	1941	3.8	1116	1627	68.60	31.40	1.28E-04	12.85
PIL165	- 30	0.03	1.67E+07	589	116	2.18	473	526	89.89	10.11	3.15E-05	3.16
PIL162		0.05	2.80E+07	2399	622	2.41	1777	2035	87.32	12.68	7.27E-05	7.29
PIL164		0.07	1.87E+07	1515	446	2.49	1069	1248	85.65	14.35	6.67E-05	6.69
PIL166		0.12	2.94E+07	6036	3238	2.83	2798	3942	70.98	29.02	1.34E-04	13.45
PIL268		0.21	4.97E+07	8215	3612	2.81	4603	5888	78.17	21.83	1.18E-04	11.88

[1] Total area of grains in 2-D EBSD map.

[2] Total number of grains with misorientation differences lower than 10°.

[#] co-ordination = number of grains within 1 mm misoriented by less than 10°

[3] $\text{Number of unique grains} = (\text{Number of grains in 2-D}) - (\text{Number of non-unique grains})$

[4] $\text{Number of "distinct" grains in 2-D} = \text{Number of unique grains} + \frac{\text{Number of non-unique grains}}{\text{Average co-ordination}}$

[5] $\text{Percentage of unique grains in 2-D} = 100 \times \frac{\text{Number of "distinct" grains in 2-D}}{\text{Total Number of .grains in 2-D}}$

[6] $\text{Percentage of repeat counted grains in 2-D} = 1 - \text{Percentage of unique grains in 2-D}$

[7] $\text{Number density of "distinct" grains} = \frac{\text{Number of "distinct" grains in 2-D}}{Area}$

[8] $\text{Number density of "distinct" grains as ratio to starting material} = \frac{\text{Number density of "distinct" grains}}{\text{Number density of "distinct" grains within undeformed sample}}$

Deformed ice grains might have intragranular distortions, which are presented as misorientation changes within grains. Therefore, internal distortion might affect the calculation results using mean orientation. Figure S4 shows the distribution of mis2mean (misorientation between each pixel and the mean orientation of its parent grain) values for each sample. The distribution of mis2mean for all deformed samples are skewed, with a peak at a smaller mis2mean value and a tail extending to higher mis2mean values. For all samples except PIL268 (12% strain, -30 °C), 95% of mis2mean values are lower than 10°. The mean and median mis2mean values are all lower than 5° (Table S3).

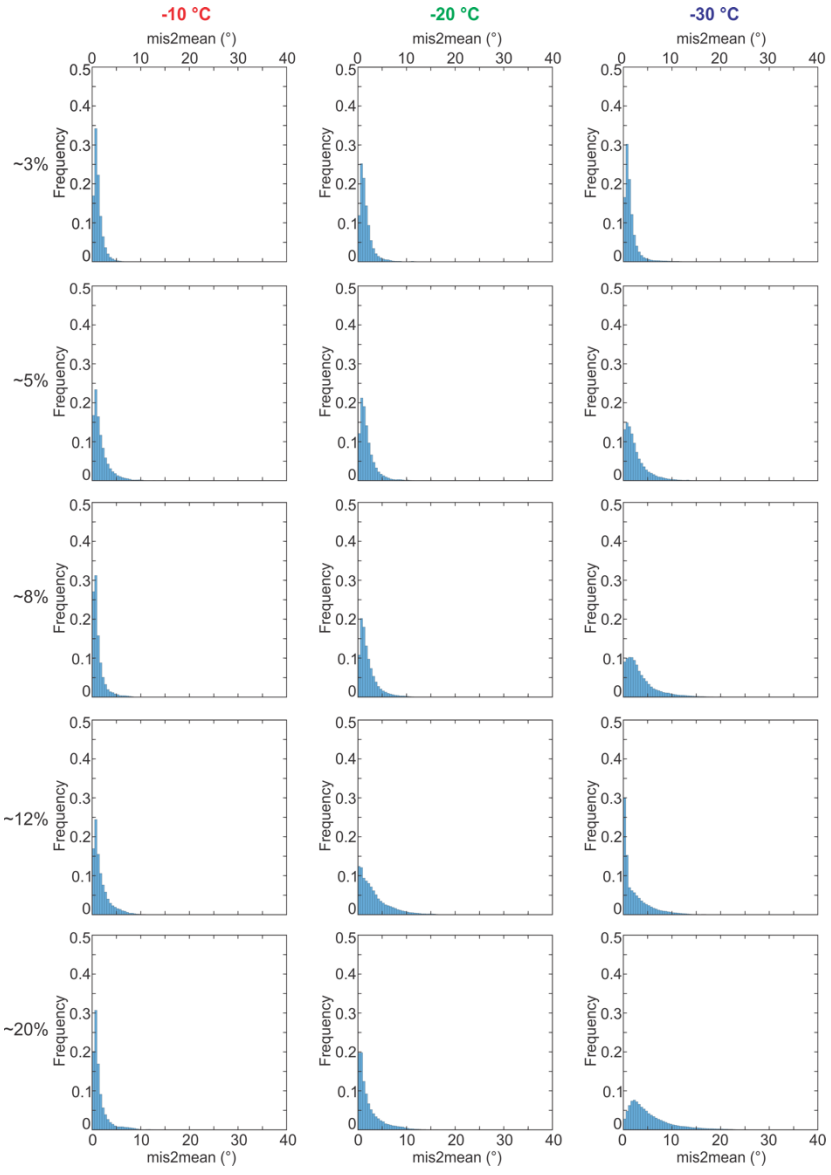

Figure S4. Distribution of mis2mean values for all deformed samples

Table S3 Summary of statistics of mis2mean values

Sample number	Statistics of mis2mean values (degree)					
	95% are smaller than	Mean	Max	Median	Lower quartile	Higher quartile
PIL176	3	1.23	12.38	0.98	0.61	1.55
PIL163	5.5	1.84	19.78	1.28	0.66	2.38
PIL178	4	1.28	15.5	0.83	0.47	1.53
PIL177	6	1.91	18.87	1.25	0.64	2.48
PIL007	6	1.65	17.07	0.98	0.57	1.87
PIL254	4.5	1.69	18.03	1.28	0.76	2.08
PIL182	5	1.9	21.04	1.43	0.81	2.42
PIL184	5.5	2.07	19.97	1.54	0.86	2.7
PIL185	10	3.46	38.69	2.45	1.02	4.73
PIL255	8.5	2.47	27.29	1.4	0.61	3.2
PIL165	4	1.48	24.17	1.06	0.64	1.76
PIL162	7.5	2.54	23.49	1.83	0.89	3.36
PIL164	10	3.52	31.69	2.57	1.3	4.63
PIL166	9.5	2.68	36.13	1.33	0.43	3.72
PIL268	15.5	5.59	56.3	4.12	2.24	7.32

Section S5 Test of the influence of grain size threshold on the CPO of "small" grains

Figure S5 shows a comparison of contoured stereonets of *c*-axes of "big" and "small" grains in samples deformed at -10, -20 and -30 °C to ~12% strain. The grain size thresholds chosen are: mean grain size, SMR (square mean root) grain size, median grain size and peak grain size. We use M-index values to quantify the strength of the CPOs. The M-index values are similar for "big" or "small" grains separated by different grain size thresholds. This observation suggests the grain size threshold used to distinguish "big" and "small" grains does affect the observation in a significant way.

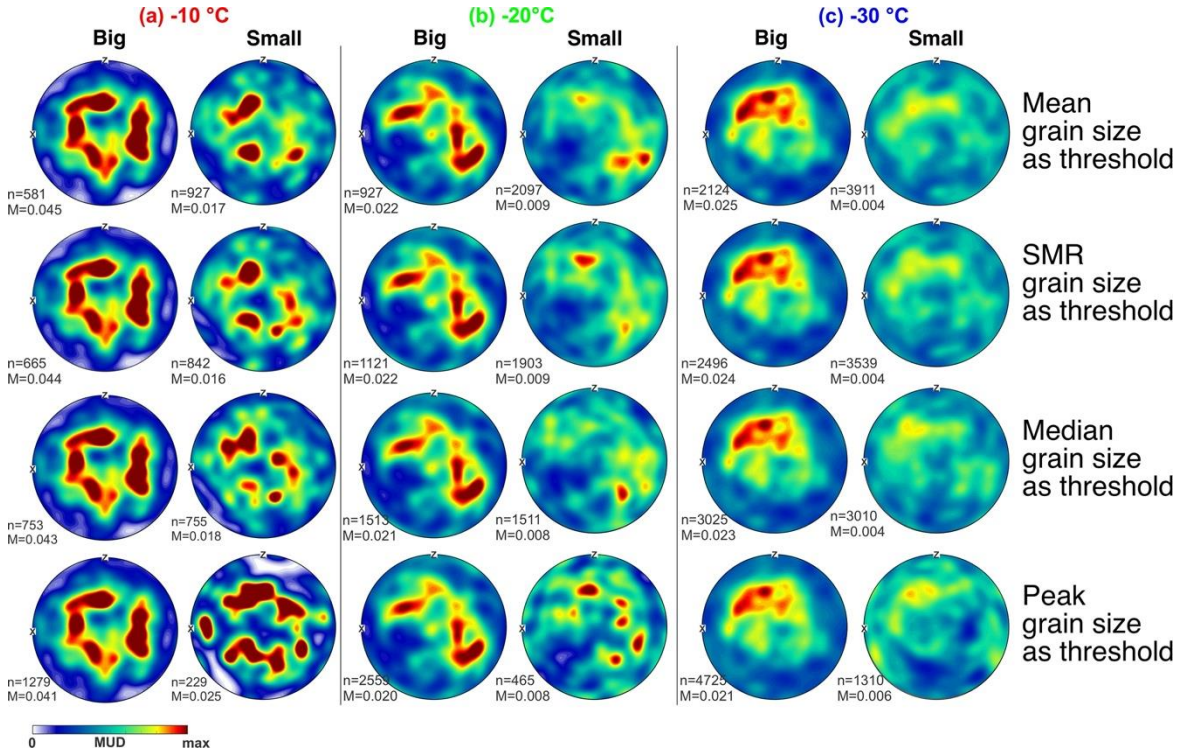

Figure S5. The contoured *c*-axis CPOs of "big" and "small" grains in samples deformed at **(a)** -10, **(b)** -20 and **(c)** -30 °C to ~12% strain. "Big" and "small" grains are separated using the threshold of mean grain size (row 1), SMR (square mean root) grain size (row 2), median grain size (row 3) and peak grain size (row 4). Number of grains and M-index value are marked at the bottom left corner of the corresponding *c*-axis CPO.

Section S6 Estimation of activation energy, Q, from the mechanical data in this study

The relation between activation energy, Q, and strain rate, $\dot{\varepsilon}$, is:

$$\dot{\varepsilon} = A\sigma^n \exp\left(-\frac{Q}{RT}\right), \qquad \text{(Equation S17)}$$

where A is a material-dependent parameter ($MPa^{-n}m^p s^{-1}$), σ is the measured bulk stress (MPa), n is the stress exponent, Q is the activation energy ($kJmol^{-1}$), R is the gas constant ($= 8.314 \times 10^{-3}\ kJmol^{-1}K^{-1}$) and T is the absolute temperature (K). Note grain size effect is not considered in this calculation.

Q can be calculated directly from constant stress experiments at different temperatures. However, calculation of Q from a set of constant rate experiments requires that the stress exponent (n) is known. We do not have values of n from the experiments published here, so we use values of 3 and 4 that span the range from peak stress to flow stress for similar experiments at -10

°C (Qi et al., 2017). A peak stress n values of 4.1 was derived for similar experiments at -30 °C (Craw et al., 2018). For calculation purposes we generate a modelled strain rate, $\dot{\varepsilon}_m$, that relates to a normalised stress value. The modelled strain rate, $\dot{\varepsilon}_m$ and $\dot{\varepsilon}$ have the following relationship:

$$\frac{\dot{\varepsilon}}{\dot{\varepsilon}_m} = \frac{\sigma^n}{\sigma_{norm}^n}, \qquad \text{(Equation S18)}$$

where σ_{norm} is the normalised stress and it is set to 1.

We calculated $\dot{\varepsilon}_m$ using measured bulk stress and strain rate data at peak stress or at a final strain of ~20% using n=3 or n=4. Q values are calculated from the fit to an Arrhenius plot of log ($\dot{\varepsilon}_m$) as a function of 1/T as shown in Fig. S6. The slope of linear fit is the *-Q/(2.3R)*.

Best fit to all data (-10, -20 and -30C) give activation energies of 98 kJ/mol and 103 kJ/mol from peak and final stress data assuming n=3 and 131 kJ/mol and 138 kJ/mol from peak and flow stress data assuming n=4. These values are close to reported *Q* values of 71-124 kJ/mol (-5 °C- -30 °C) from Budd and Jacka (1989) and ~133 kJ/mol (-1.5 °C- -12.8 °C) from Glen (1955) and 64-250 kJ/mol from Kuiper and others (2019). Note experiments in this study only covers three temperature values. Hence, the calculated *Q* values have large uncertainties. More data points are needed for a better *Q* investigation.

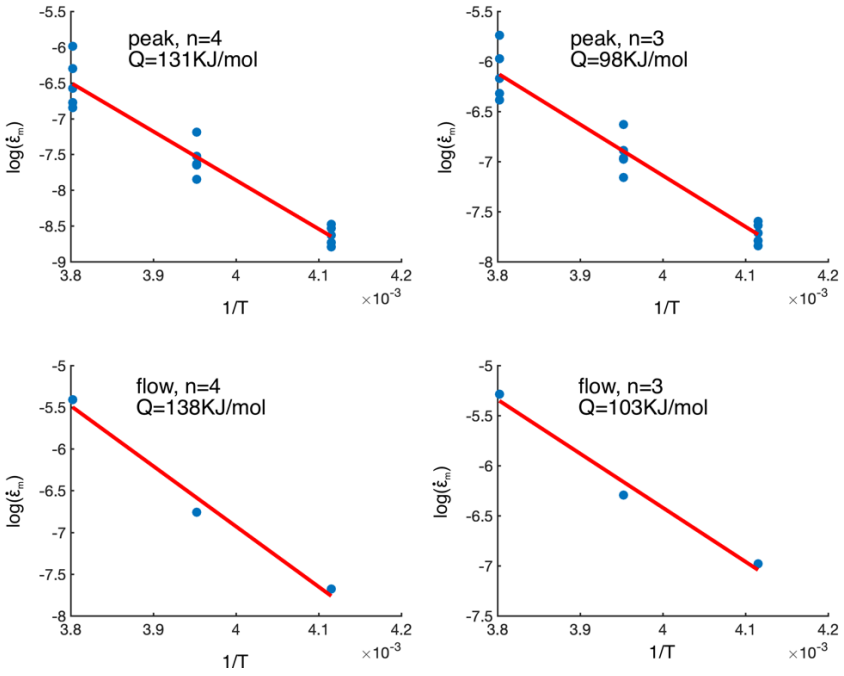

Figure S6. Arrhenius plot illustrating the activation energy, *Q*.